Available online at www.sciencedirect.com

ScienceDirect

IFAC Papers Online CONFERENCE PAPER ARCHIVE

IFAC PapersOnLine 52-14 (2019) 129–134

Limitations on control performance in the Czochralski crystal growth process using bright ring measurement as a controlled variable ⋆

Halima Zahra Bukhari * **Morten Hovd** * **Jan Winkler** **

* *Department of Engineering Cybernetics, NTNU, Trondheim, Norway (e-mail: halima.bukhari@ntnu.no; morten.hovd@ntnu.no).*
** *Institute of Control Theory, Faculty of Electrical & Computer Engineering, TU Dresden, Germany, (e-mail: jan.winkler@tu-dresden.de)*

Abstract: This paper develops a dynamical model for crystal diameter in the Czochralski process for production of monocrystalline silicon. The model combines simplified crystal growth dynamics with rigorous ray tracing to describe the camera image used for diameter control, and it is demonstrated that the resulting model captures the so-called *measurement anomaly* that represents a key performance limitation for crystal diameter control.

Keywords: Czochralski process, bright ring measurement, right half plane zero, ray tracing, interface dynamics

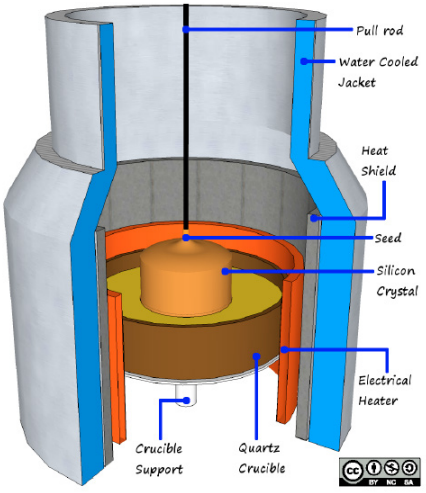

Fig. 1. Assembly of a typical CZ puller. (This figure is licensed under a Creative-Commons BY-NC-SA license) (Rahmanpour, 2017)

1. INTRODUCTION

The Czochralski (CZ) process is a commercial process for the growth of single crystals of semiconductors (e.g., silicon, germanium and gallium arsenide), metals, salts and synthetic gemstones. This process is the workhorse for the mass production of mono-crystalline silicon ingots, which are later used as base material (substrate or wafer) in semiconductor and photovoltaic industries.

A typical CZ furnace assembly is shown in Fig. 1. In this process, high purity silicon is melted in a crucible which is surrounded by annular and base heaters. When the desired melt temperature is attained, a seed crystal mounted at the end of a pulling rod is immersed into the molten silicon, and then gradually pulled upwards. This pulling forms a meniscus between the growing crystal and the molten silicon, and this meniscus protrudes above the level of the melt. Heat loss at the top of the meniscus causes the molten silicon to solidify (crystallize), and when the pulling rate and crystal growth rate is well balanced it is possible to produce a crystal of constant radius. While there are several phases of this crystal growth process, this paper addresses modeling for diameter control in the so-called *body phase*, *i.e.*, the main part of the process where a constant crystal radius is desired. The manipulated variable for radius control is the pulling speed, while this work will focus on the use of a radius measurement derived from a camera image.

The high temperatures inside the growth chamber lead to the formation of a glowing ring near the base of the crystal, because light from glowing hot surroundings gets reflected by the meniscus before entering the camera. The camera is calibrated to aim at the meniscus to measure the radius of a specific glowing ring formed on the meniscus (in the vicinity of melt-crystal/three-phase boundary). This glowing ring is referred to as the *bright ring* in Czochralski growth parlance. In reality, the perspective occlusion due to the growing crystal in the centre and the surrounding heat shield prevents the full 360° view of the bright annular ring by the camera. Throughout this process, the crucible is gradually lifted upwards to maintain the melt surface at a constant level. In this way, the camera continues to aim at the meniscus thereby avoiding any need to vary the camera location or focus during the entire growth process.

⋆ The work is funded by the Norwegian Research Council's ASICO project 'project No. 256806/O20'

10.1016/j.ifacol.2019.09.176

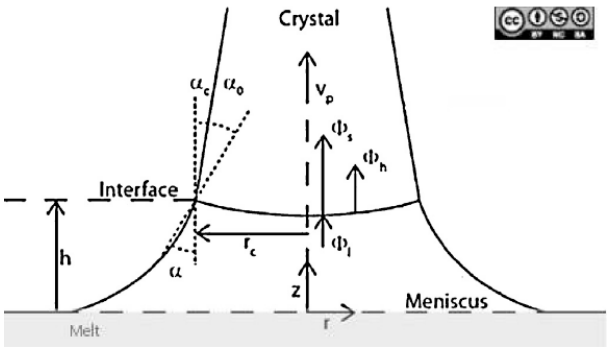

Fig. 2. Schematic view of the melt-crystal interface. (This figure is licensed under a Creative-Commons BY-NC-SA license) (Rahmanpour, 2017)

From an economical viewpoint, it is highly desirable to maintain the radius of the produced crystal as constant as possible. This allows for minimal post grinding or material cut off, thereby making the overall process cost effective.

1.1 Measurement anomaly

An important system state for a commercial CZ process, as explained above, is the radius of the growing crystal, which unfortunately cannot be measured directly. Instead, the radius measurement of the bright ring is used for the diameter control (Digges et al., 1975), (Duffar, 2010) of the crystal ingots in case of Si crystal growth.

An alternative measurement method is the continuous weight measurement of the growing ingot. An *anomaly, i.e., an inverse response* in the weight measurement signal was first reported by Bardsley et al. (1974) in the year 1974 and later on by some of the fellow authors in the year 1977 (Bardsley et al., 1977a), (Bardsley et al., 1977b).

A fact that did not get such a broad attention in literature is that the bright ring measurement is also affected by a similar anomaly. With a decrease in pulling speed the meniscus height decreases, making the meniscus profile flatter. This causes the bright ring to initially move inwards before an increase in crystal radius (as reported in Gevelber et al. (1988) and Gevelber (1994)). This effect will cause the optical radius sensing method to indicate that the crystal radius initially moves in the opposite direction of what it actually does, thereby producing the so called *anomalous behaviour* also for the camera measurement. For the sake of clarity and to illustrate the use of some nomenclature, the melt-crystal interface is schematically depicted in Fig. 2.

The paper is organised as follows. Section 2 describes the crystal diameter dynamics of the CZ process. The measurement model used to simulate the bright ring and the associated anomolous behavior is explained in section 3. Model linearization and the anaysis of the right half plane zeros is discussed in section 4, followed by conclusions.

2. PROCESS MODEL

The model considered here is a simplified model aiming at capturing only the dynamics of the crystal radius and the pulling rate as control input. Therefore, the slower dynamics of the crystal melt temperature is neglected. The model therefore covers only the crystal radius, the heat balance at the melt-crystal interface, and the dependency of the radius on the meniscus height.

We therefore get the following simplified model of the CZ growth process (also referred to as a hydromechanical-geometrical model or simply interface dynamics):

$$\dot{r}_c = v_g \tan(\alpha_c) \tag{1a}$$

$$\dot{h}_c = v_p - v_g \tag{1b}$$

$$\alpha_c = \arcsin\left\{1 - \left(\frac{h_c}{a}\right)^2 \left[1 + 0.6915\left(\frac{r_c}{a}\right)^{-1.1}\right]\right\} - \alpha_0 \tag{1c}$$

where r_c is the crystal radius, h_c is the height of the meniscus at the three-phase boundary, v_g is the growth rate of the crystal (lengthwise) calculated from the thermal models explained in section 2.1, v_p is the pulling speed, and α_c is the cone angle at the interface, which can be mathematically expressed as the rate of change in crystal radius w.r.t. change in the crystal length, i.e., $\alpha_c = \frac{\mathrm{d}r_c}{\mathrm{d}l}$. The expression of α_c in (1c) is derived from the analytical approximation of meniscus height h_c given by Johansen (1994). Note the difference between α_c and the contact angle α, which are related through $\alpha = \alpha_0 + \alpha_c$, where α_0 is the contact angle (*wetting angle* in some branches of science) at constant radius growth. The parameter a is the Laplace constant, also termed the *capillary length*. We will assume $\alpha_0 = 11°$ (Tatarchenko (1993), Rahmanpour et al. (2017)), and $a = 7.62\,\mathrm{mm}$. The derivative of meniscus height expressed in (1b) assumes perfect compensation for melt level changes through crucible lift.

2.1 Thermal model assumptions for crystal growth rate

The crystal growth rate is found from an energy balance at the interface:

$$v_g = \frac{\phi_s - \phi_l}{\rho_s \Delta H} \tag{2}$$

where ϕ_s is the heat flux from the interface into the crystal, ϕ_l is the heat flux from the melt to the interface, ρ_s is the density of the solid crystal, and ΔH is the heat of fusion of silicon.

The heat flux is assumed to have a constant value, i.e., $\phi_s = 1.3 \times 10^5\,\mathrm{W\,m^{-2}}$ (Rahmanpour et al., 2016).

Since the crystal gradually protrudes longer into the cooler areas above the heat shield, the assumption of a constant ϕ_s clearly cannot hold over the timespan of the entire body stage. However, it is a reasonable assumption over the much shorter timescale of the measurement anomaly. For the heat flux ϕ_l from the melt to the interface, two different model assumptions will be investigated:

Model I: Assuming heat transfer within the meniscus itself is dominated by conduction (model assumption I) leads to the following approximation of the heat flux (Hurle et al., 1990):

$$\phi_l = \frac{k_l}{h}(T_B - T_S) \tag{3}$$

where T_B is the temperature at the base of the meniscus and T_S is the temperature at the interface (the melting

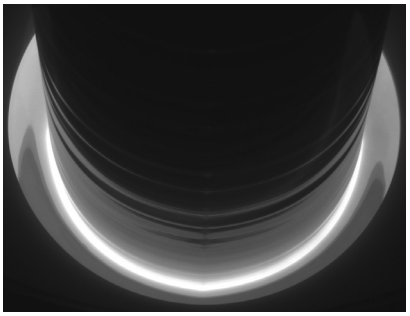

Fig. 3. Actual plant image from the CCD camera

point of silicon). According to Yamasue et al. (2002), the average thermal conductivity k_l of molten silicon at 1700 K is around $57\,\mathrm{W\,m^{-1}\,K^{-1}}$. Using the data from Rahmanpour et al., a heat flux of $\phi_l = 46\,000\,\mathrm{W\,m^{-2}}$ for a meniscus height $h_c = 7\,\mathrm{mm}$ then yields $T_B - T_S \approx 5.6\,\mathrm{K}$. This implies that the temperature within the melt is not uniform - Rahmanpour had a 31 K temperature difference between the bulk of the melt and the interface. To make this consistent with the heat flux to the interface, a significant part of the thermal resistance needs to be between the bulk of the melt and the base of the meniscus (since it is not reasonable to have a lower heat transfer rate in the meniscus than that resulting from pure conduction). To maximize the difference between the two model assumptions, it will here be assumed that T_B is constant, independent of meniscus height.

Model II: Assuming that the heat transfer from the melt to the interface is dominated by convection, and is independent of meniscus height. This leads to a constant ϕ_l and hence a constant growth rate v_g (when neglecting the slow dynamics of the melt temperature). This model assumption is the one used by Rahmanpour et al. (2017).

3. MEASUREMENT MODEL

A typical video image of the glowing meniscus around the growing crystal captured by a camera installed at a viewing port of a commercial puller is shown in Fig. 3. Note that since the contrast between the meniscus and the solid crystal is very weak, the camera measurement does not try to measure the crystal radius directly, but rather some identifiable point on the bright ring slightly outside the actual solid crystal. It is this inability to directly measure the crystal radius that causes the so-called 'bright ring anomaly' - which in linear control parlance is a *right half plane transmission zero* of the corresponding transfer function from the pulling speed to the radius measurement - that is the object of study in this work.

The resulting illuminated profile for the meniscus can be calculated by

- ✓ Calculating the meniscus shape. This can be calculated from the so-called Laplace-Young equation. Unfortunately, there is no analytical solution to the Laplace-Young equation, which therefore has to be solved numerically (Huh and Scriven, 1969). In this work, the analytical approximation given by Hurle (1983) is used instead:

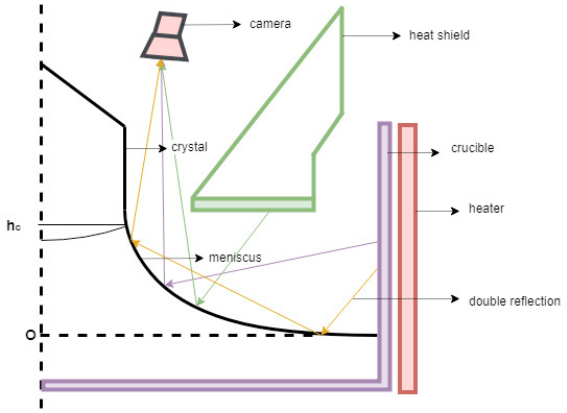

Fig. 4. Ray tracing set up showing incident and reflected light rays within the growth furnace (This figure not drawn to scale)

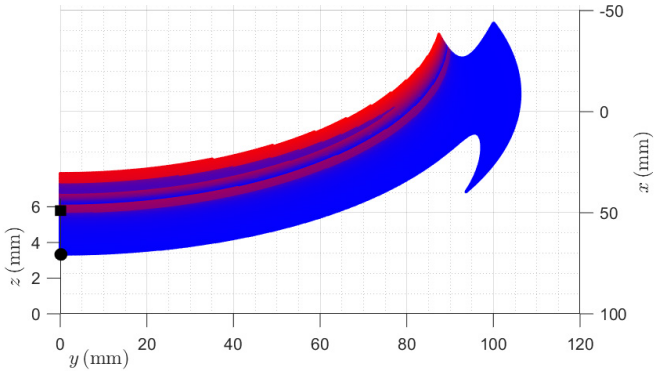

Fig. 5. Theoretically calculated brightness profile as observed by the camera. Minimum brightness (blue); maximum brightness (red). Since, the view is symmetric on either side of the xz [1] -plane/camera plane, the left portion of the meniscus is not shown.

$$r(h_c, r_c, z) = r_c + \sqrt{\frac{2}{A} - h_c^2} - \sqrt{\frac{2}{A} - z^2} - \frac{1}{\sqrt{2A}} \ln\left[\frac{z}{h_c} \cdot \frac{\sqrt{2} + \sqrt{2 - A \cdot h_c^2}}{\sqrt{2} + \sqrt{2 - A \cdot z^2}}\right] \tag{4}$$

where r and z are the radial and vertical coordinates of the meniscus surface respectively. The meniscus surface extends from the three-phase boundary (r_c, h_c) to the crucible wall $(R_{cru}, 0)$ such that $r \in [r_c, R_{cru}]$, $z \in [0, h_c]$ where R_{cru} is the crucible radius. A is defined as:

$$A = \frac{1}{a^2} + \frac{\cos(\alpha)}{2 r_c\, h_c}$$

- ✓ Tracing rays backwards from the camera, via some chosen point on the meniscus, back to its origin either on the crucible wall or the underside of the heat shield. A simple ray-tracing set up is illustrated in Fig. 4.
- ✓ A measure of (relative) brightness can be obtained by perturbing a point on the meniscus, and calculating the resulting perturbation of the emission point on

[1] The x and y axes in Fig. 5 define the radial coordinates of the meniscus, i.e., $r = \sqrt{x^2 + y^2}$, while z-axis represents the height of the meniscus above the melt surface.

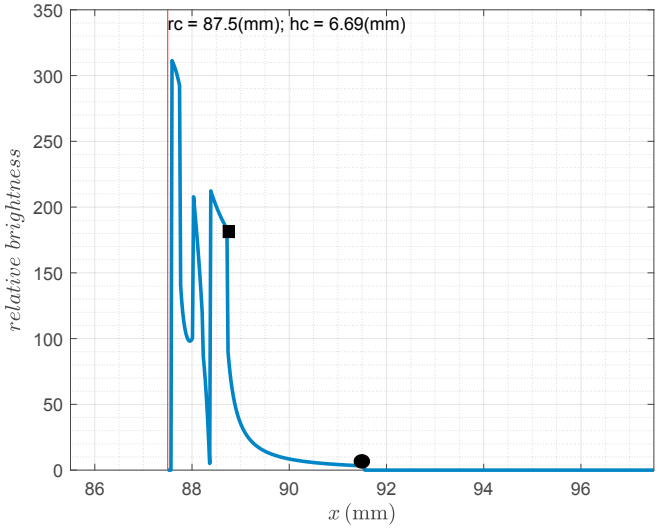

Fig. 6. Relative brightness profile as observed along the longitudinal/camera plane

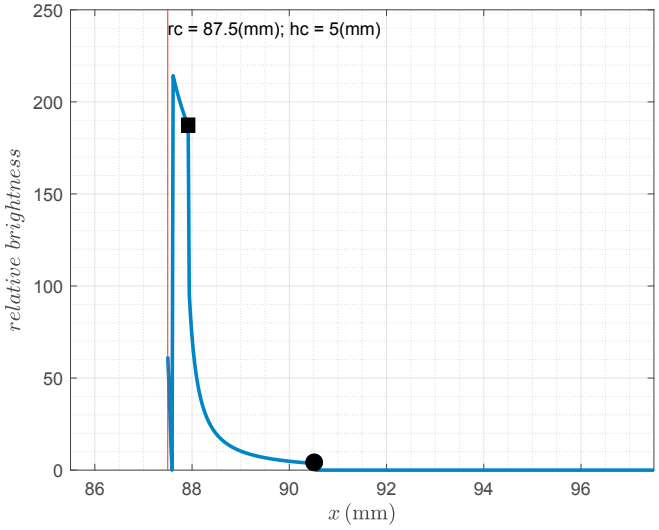

Fig. 7. Relative brightness profile as observed along the longitudinal/camera plane, for low meniscus height

the light source (crucible wall or underside of heat shield), while also accounting for both the viewing angle of the emission point of the light source as seen from the point on the meniscus as well as the emission intensity of the light source emission point in question.

The full details of this procedure will not be presented here due to space limitations. The procedure sketched above can be extended by considering multiple reflections on the melt surface between the emission point and the camera. This results in a calculated brightness profile as illustrated in Fig. 5.

The calculated brightness profile in Fig. 6 shows the brightness profile along the portion of the illuminated meniscus in the plane of the camera.

Furthermore, when visually comparing the 2D relative brightness profile in Fig. 6 calculated for the meniscus orientation in the plane of the camera with the 3D calculated brightness profile in Fig. 5, it becomes clear that the fluctuations in the left part of Fig. 6 correspond to bright bands close to crystal ingot in Fig. 5. However, the similar bright bands are not evident in video images from a production plant Fig. 3. There can be several reasons for this discrepancy, such as:

- ▷ The most probable cause is noise or surface waves resulting in blurring/spatial averaging of the brightness profile.
- ▷ Saturation of the image sensor of the camera, effectively cutting of the highest peaks in the brightness profile. This will depend on the exposure control of the camera.

However, two points on the brightness profile can be reliably identified from the camera images:

(1) The illuminated point marked as '■' in Figs. 5 or 6, orginates from the highest point on the crucible wall whose reflection from the meniscus can be seen by the camera (that is not obstructed by the heat shield).

(2) The point corresponding to the circle '●' in Figs. 5 or 6, orginating from the innermost edge of the underside of the heat shield.

Either of the two points marked in Figs. 5 and 6 may be used as a basis for the bright ring radius measurement. Further justification for not using the the peak value of the brightness profile as a measure of crystal radius can be found from Fig. 7. This figure shows the calculated brightness profile for a low meniscus height. It is observed that the features in the left part of the figure in Fig. 6 have disapeared. This would mean that if one were to base the radius measurement on the brightest point on the profile, one would risk this measurement to change discontinuously depending on process conditions.

In the following, the point '■' is used for the radius measurement, as this is where the change in brightness is the strongest. The corresponding radius measurement will be termed the *bright ring radius*, denoted r_{br}. To our knowledge, this is also the bright ring measurement used in industry. Note that there is an offset between the actual crystal radius and the bright ring radius measurement. At steady state this difference can be accounted for by applying a bias to the measured r_{br}.

4. LINEARIZED PLANT MODEL DYNAMICS AND ANALYSIS

The non-linear CZ dynamics expressed in (1) combined with the bright ring radius measurement r_{br} described above constitute a non-linear model relating pulling speed to bright ring radius. Linearizing this non-linear model, the resulting linear model can be expressed in general form as

$$\begin{aligned} \dot{x} &= Ax + Bu \\ y &= Cx \end{aligned} \tag{5}$$

Note that we do not here include a direct throughput term from input u to output y, as the measurement only depends on the states.

Based on the two thermal model assumptions (as discussed in section 2), the non-linear plant dynamics (1)

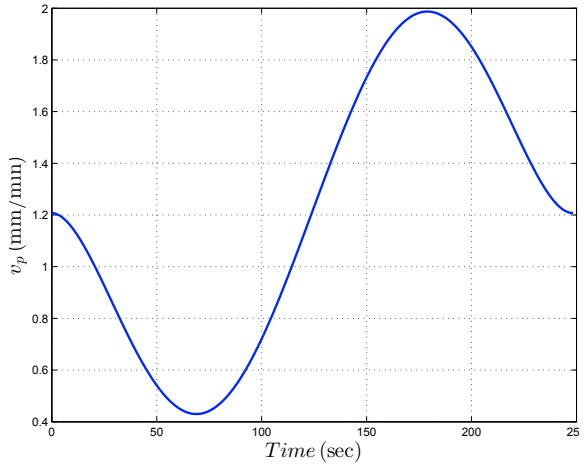

Fig. 8. Applied pull speed profile

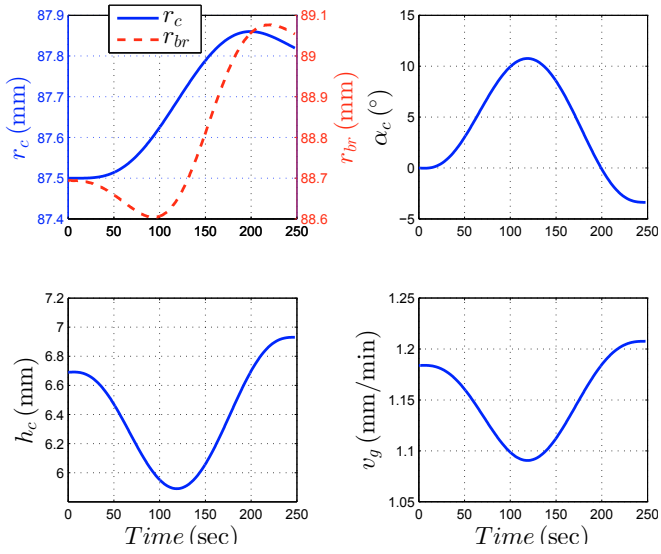

Fig. 9. Non-linear plant response for **Model I** subjected to the applied input shown in Fig. 8, crystal radius r_c, bright ring radius r_{br} and α_c in top left- and -right panes respectively, the meniscus height and the growth rate in the bottom left- and right-panes respectively

are simulated for a specific input profile as shown in Fig. 8. The resulting responses for the first and second model assumptions (first: heat transport within the melt itself is dominated by conduction; second: heat transport from melt to interface is dominated by convection), i.e., system states, bright-ring radius measurement, meniscus height and growth-rate are illustrated in Figs. 9 and 10 respectively. The inverse reponse or non-minimum phase behaviour in the bright ring measurement is quite evident. Moreover, it can be seen that for the second assumption that relates to convection dominated heat transfer within the melt, the growth rate (v_g) remains constant whereas it varies for the heat transfer assumption based on conduction.

The linear models thus obtained possess right half plane (RHP) zero in the bright ring radius measurement transfer function, thereby confirming the non-minimum phase behavior as discussed in section 1.1. In order to authenticate

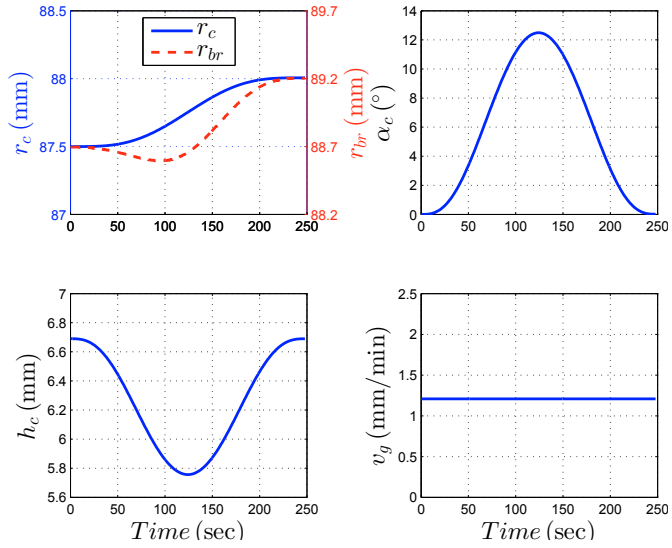

Fig. 10. Non-linear plant response for **Model II** subjected to the applied input shown in Fig. 8, crystal radius r_c and bright ring radius r_{br}, α_c in top-left and -right panes respectively, the meniscus height and the growth rate in the bottom-left and right-panes respectively

Table 1. Pole and zero locations for the linearized models I and II

Model Assumption I *s-plane* location [rad/sec]			Model Assumption II *s-plane* location [rad/sec]		
Zero	Pole 1	Pole 2	Zero	Pole 1	Pole 2
0.02128	8.78e-06	-1.684e-3	0.02183	4.63e-07	7.602e-06

the linearization process, the responses of the non-linear and linearzied models are compared by exciting both non-linear as well as linear models with the same applied input. Consequently, the input as shown in Fig. 8 is applied to both linear and non-linear models and the resultant system responses for thermal models I and II is shown in Fig. 11. Another comparison between the non-linear and linear models is obtained by using the step perturbation of $1\,\mathrm{mm\,min^{-1}}$ in pull-speed to both linear and non-linear models. The response of measured bright ring radius to the step perturbation at steady state is shown in Fig. 12 for the thermal model assumption I. Since the bright ring radius response to step perturbation for thermal model II is practically indisntinguishable from that of thermal model I and is therfore not shown in Fig. 12. The close agreement between the non-linear and linear model response, especially in the initial non-minimum phase response, confirms the validity of the obtained linear models.

The analysis of the linearized models (with poles and zeros listed in Table 1), shows that the location of RHP zeros does not depend much on the assumption of heat transfer method from the melt into the crystal.

The RHP zero will put an upper bound on the achievable closed loop bandwidth for the control of crystal radius, whereas the RHP pole(s) put a lower bound on the required bandwidth (Skogestad and Postlethwaite, 2007). Moreover, the RHP zero and RHP pole(s) are separated by more than three orders of magnitude, indicating that acceptable control quality should be obtainable.

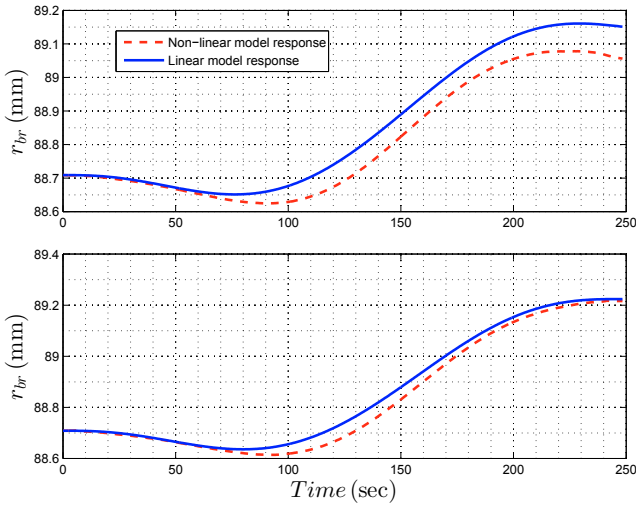

Fig. 11. Comparison of non-linear and linear system dynamics for thermal models I (top row) and II (bottom row), when excited by the input profile as shown in Fig. 8.

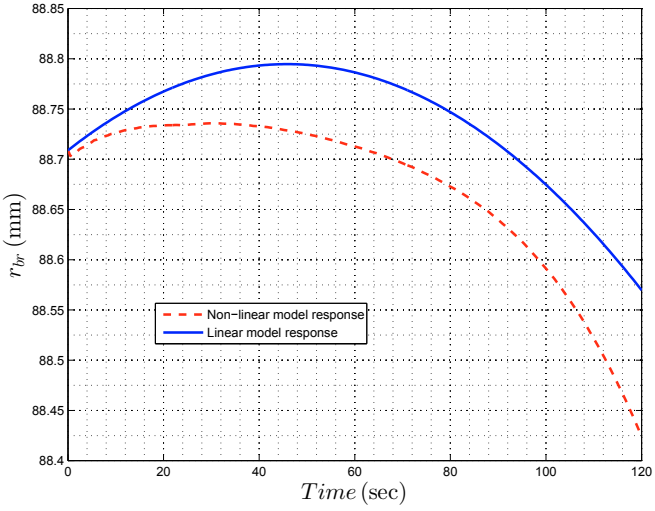

Fig. 12. Comparison of non-linear and linear system dynamics for thermal model I, when excited by step perturbation in v_p.

5. CONCLUSIONS

The paper develops a simple model for the crystal radius control problem in the CZ process for the production of monocrystalline silicon. The model combines a simplified crystal growth model with rigorous ray tracing to obtain the bright ring radius measured by the camera. It is shown that this simplified model can capture the non-minimum phase characteristics of the plant, and that these non-minimum phase characteristics do not depend strongly on how heat transfer from the melt to the crystal is modelled. Future work will investigate the control of the crystal radius r_c (as opposed to controlling the bright ring radius r_{br}) based on the simple model derived in this paper.

REFERENCES

Bardsley, W., Cockayne, B., Green, G., Hurle, D., Joyce, G., Roslington, J., Tufton, P., Webber, H., and Healey, M. (1974). Developments in the weighing method of automatic crystal pulling. *Journal of Crystal Growth*, 24, 369–373.

Bardsley, W., Hurle, D., and Joyce, G. (1977a). The weighing method of automatic Czochralski crystal growth: I. basic theory. *Journal of Crystal Growth*, 40(1), 13–20.

Bardsley, W., Hurle, D., Joyce, G., and Wilson, G. (1977b). The weighing method of automatic Czochralski crystal growth: II. control equipment. *Journal of Crystal Growth*, 40(1), 21–28.

Digges, T., Hopkins, R., and Seidensticker, R. (1975). The basis of automatic diameter control utilizing "bright ring" meniscus reflections. *Journal of Crystal Growth*, 29(3), 326–328.

Duffar, T. (2010). *Crystal growth processes based on capillarity: Czochralski, Floating zone, shaping and crucible techniques*. John Wiley & Sons.

Gevelber, M.A. (1994). Dynamics and control of the Czochralski process III. interface dynamics and control requirements. *Journal of Crystal Growth*, 139(3-4), 271–285.

Gevelber, M.A., Stephanopoulos, G., and Wargo, M.J. (1988). Dynamics and control of the Czochralski process II. objectives and control structure design. *Journal of Crystal Growth*, 91(1-2), 199–217.

Huh, C. and Scriven, L. (1969). Shapes of axisymmetric fluid interfaces of unbounded extent. *Journal of Colloid and Interface Science*, 30(3), 323–337.

Hurle, D. (1983). Analytical representation of the shape of the meniscus in Czochralski growth. *Journal of Crystal Growth*, 63(1), 13–17.

Hurle, D., Joyce, G., Ghassempoory, M., Crowley, A., and Stern, E. (1990). The dynamics of Czochralski growth. *Journal of Crystal Growth*, 100(1-2), 11–25.

Johansen, T.H. (1994). An improved analytical expression for the meniscus height in Czochralski growth. *Journal of Crystal Growth*, 141(3-4), 484–486.

Rahmanpour, P. (2017). *Model-based Control of the Czochralski Silicon Crystal Pulling Process*. Ph.D. thesis, Department of Engineering Cybernetics, NTNU.

Rahmanpour, P., Sælid, S., and Hovd, M. (2017). Run-to-run control of the Czochralski process. *Computers & Chemical Engineering*, 104, 353 – 365.

Rahmanpour, P., Sælid, S., Hovd, M., Grønning, O., and Jomaa, M. (2016). Nonlinear model predictive control of the Czochralski process. *IFAC-PapersOnLine*, 49(20), 120 – 125. 17th IFAC Symposium on Control, Optimization and Automation in Mining, Mineral and Metal Processing MMM 2016.

Skogestad, S. and Postlethwaite, I. (2007). *Multivariable Feedback Control: Analysis and Design*, volume 2. Wiley New York.

Tatarchenko, V. (1993). *Shaped Crystal Growth*, volume 20. Springer Science & Business Media.

Yamasue, E., Susa, M., Fukuyama, H., and Nagata, K. (2002). Thermal conductivities of silicon and germanium in solid and liquid states measured by non-stationary hot wire method with silica coated probe. *Journal of Crystal Growth*, 234(1), 121 – 131.